Arch. Metall. Mater. **69** (2024), 4, 1685-1694

DOI: https://doi.org/10.24425/amm.2024.152098

MIN YU[1*], ZHEN CHENG[2], RUI-BIN GOU[2], NIAN WANG[3]

RESEARCH ON THE NON-UNIFORM TEMPERATURE FIELD DISTRIBUTION OF Q355B STEEL FOR GRAIN STORAGE UNDER FIRE CONDITIONS

To reveal the distribution characteristics of the non-uniform temperature field of structural steel under fire conditions, Q355B steel for grain storage was taken as the research object. A multi-channel temperature detection instrument was used to monitor the temperature distribution of Q355B test plate in real time under gas fire, and the distribution characteristics of the non-uniform temperature field of the steel were studied under different heat inputs. The results showed that the temperature changes within 600 mm from the flame point were significant, while the temperature changes beyond 600 mm were not sensitive. The peak temperature T_{max} and the heating rate v_r at the fire source points of each test plate increased linearly with the increase of heat input Q at the fire source. With the increase of distance d, the variation trend of the time t_{max} for each test plate to reach the peak temperature in the rolling direction, was the same. As d increased, t_{max} gradually increased and tended to stabilize. The average cooling rates v_{d1} and v_{d2} of each test plate decreased with the increase of d. The temperature distribution patterns of each test plate were the same. The T_{max}-d curve of each test plate followed the Boltzmann function distribution, the Q-ΔT followed a linear relationship, and the Q-d_0 followed an exponential function relationship. By combining the three, a non-uniform distribution model of T_{max}-Q temperature field under gas fire was obtained.

Keywords: Q355B steel; Peak temperature; Gas fire; T_{max}-Q temperature field model

1. Introduction

With the continuous advancement of China's modernization, the use of low-carbon structural steel in various fields, such as machinery, ships, civil engineering, and agriculture, has been steadily increasing. However, the mechanical performance requirements of steel structures are becoming higher due to the increasing requirements for large-scale, long-life, and high-load service. Despite this, the service environment of steel structures is becoming increasingly complex, leading to a growing risk of fire, and the high-temperature environment caused by fires inevitably affects the mechanical performance of steel structures [1-6]. Therefore, it is of great research value to reveal the distribution characteristics of the non-uniform temperature field during fires, to evaluate the service safety performance of steel structures after a fire.

In terms of the distribution characteristics of fire temperature fields, many researchers have conducted research on building fires [7-14], tunnel fires [15-22], and structural steel fires [23-25]. In the field of building fires, Li simulated the temperature distribution patterns in long and narrow spaces, as well as in the horizontal and vertical directions, and found that along the direction of the narrow confined space, the temperature first increases and then decreases, while in the transverse direction, the temperature in the middle is higher than that on the sides [10]. In the field of tunnel fires, Jia conducted experiments on different fire source sizes and distances and found that the longitudinal temperature distribution of the tunnel ceiling follows the Forsythe exponential decay law [19]. In terms of structural steel fires, Fischer compared the structural response of steel frame building to standard fire exposure and travel fire exposure, and found that gravity columns were the first structural element to fail [23]. Charlier proposed an analytical model based on the concept of virtual solid flame, and compared the steel temperatures measured in the travel fire test of the steel frame building with the analytical temperatures. The model can take into account both representation of fire spread and steel temperature [24]. Xia found that the coupling of computational fluid dynamics with finite element analysis using temperatures through adiabatic surfaces is a universal method capable of capturing member temperatures

[1] ANHUI SCIENCE AND TECHNOLOGY UNIVERSITY, COLLEGE OF ARCHITECTURE, BENGBU 233000, CHINA
[2] ANHUI SCIENCE AND TECHNOLOGY UNIVERSITY, COLLEGE OF MECHANICAL ENGINEERING, FENGYANG 233100, ANHUI, CHINA
[3] BENGBU SPECIAL EQUIPMENT SUPERVISION AND INSPECTION CENTER, BENGBU 233000, CHINA

* Corresponding author: yum@ahstu.edu.cn

in different experiments [25]. Ren considered the temperature gradients on the member length of the steel structure exposed to local fire, studied the resistance of the uprights under local fire, and established the finite element model of the cold-formed steel storage rack uprights [26]. Researchers have discussed the thermal conduction [27], temperature response characteristics [28], and steel emissivity at high temperatures [29], but there is a relatively little research on the non-uniform temperature field distribution characteristics of structural steel during fires. Therefore, it is of great research value to study the non-uniform temperature field distribution of structural steel for revealing the deterioration mechanism of its mechanical properties.

To reveal the distribution characteristics of the non-uniform temperature field of structural steel during a fire, the paper takes Q355B structural steel for grain storage as the research object and investigates the non-uniform temperature field characteristics of steel during a fire. It provides data support for revealing the formation mechanism of mechanical properties change of steel structure after fire and realizing the sustainable utilization of steel structure after fire.

2. Experiment preparation and method for determining the heat input

2.1. Materials and test specimens

This work focuses on four pieces of Q355B steel plate with dimensions of 1500 mm (length) × 210 mm (width) × 6 mm (thickness) in the rolling direction. The chemical compositions of the material is shown in TABLE 1.

TABLE 1

Chemical composition of Q355B steel (%)

C	Si	Mn	P	S	Cr	Ni	Cu
0.16	0.14	0.66	0.016	0.009	0.04	0.02	0.03

2.2. Method for conducting the fire simulation test

In order to reveal the distribution characteristics of the post-fire non-uniform temperature field of Q355B steel, Firstly, a gas stove is used to simulate the fire environment of structural steel. Secondly, a multi-channel temperature detection instrument is used to monitor the temperature changes of the steel during the gas fire. Thirdly, the temperature changes at various temperature measurement points on the steel plate were analyzed to reveal the non-uniform temperature field distribution characteristics of the steel plate under different heat. Finally, based on the distribution characteristics of the temperature field, a non-uniform temperature field distribution model for Q355B steel plate under gas fire is constructed, providing the theoretical support for revealing the degradation mechanism of the mechanical performance of structural steel during a fire.

Gas-fire tests were conducted on four specimens #1, #2, #3, and #4, as given in Fig. 1. The test process consists of two stages: heating for 20 minutes and then natural cooling. The tests were conducted in a windless indoor environment, and the heat input Q of the specimen was controlled by adjusting the gas stove's air inlet valve. The temperature variation of each specimen was measured in the rolling direction using a multi-channel thermometer. Nine temperature measurement points were evenly distributed along the rolling direction of the specimen, with distances from the flame center at 0, 160, 320, 480, 640, 800, 960, 1120, and 1280 mm, as shown in Fig. 2.

Fig. 1. The fire test results for each test plate

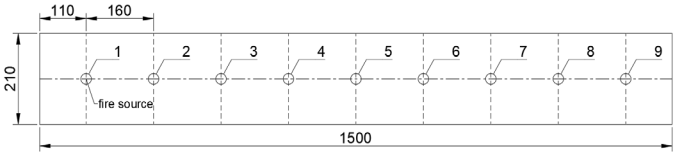

Fig. 2. The distribution of fire sources and temperature measurement points (unit: mm)

2.3. Method for determining the heat input *Q*

The heat input Q per minute to the temperature measuring point #1 at the heat source is determined using:

$$Q = C\rho Vv \tag{1}$$

Where C represents the specific heat capacity of the steel plate in J/(kg·°C); ρ represents the density of the steel plate in kg·m^3; $\boldsymbol{v}$ is the average temperature rise rate at the measuring point of the heat source within 20 minutes in °C·min^{-1}; V represents the volume at the measuring point of the heat source in m^3.

According to GB 51249-2017, the specific heat capacity C of the test plate is taken as 600 J/(kg·°C) [30]; the density ρ is taken as 7850 kg·m^3; the average heating rate v is determined by $T_{20\text{min}}$ on the temperature change curve at the heat source. The volume V is calculated based on the diameter of the thermocou-

ple probe (1 mm) and the thickness of the steel plate (6 mm), resulting in a value of 4.71×10^{-9} m^3.

The results for the peak temperature T_{max}, time required to reach the peak temperature t_{max}, temperature at the heat source after 20 minutes T_{20min}, average temperature rise rate $\boldsymbol{v}$, and heat input Q, for the fire source points of each test plate, are shown in TABLE 2.

TABLE 2

Results of the relevant parameters for the heat input Q per minute for the fire source points of each test plate

Parameter name	#1 plate	# 2 plate	#3 plate	#4 plate
T_{max} (°C)	697.72	321.68	249.33	234.78
t_{max} (min)	20.10	20.37	20.55	20.42
T_{20min} (°C)	696.53	319.18	247.47	233.71
v (°C·min^{-1})	34.83	15.96	12.37	11.69
Q (J·min^{-1})	0.77	0.35	0.27	0.26

From Fig. 3, it can be observed that the temperature distribution pattern along the rolling direction is the same for the four test boards. Regardless of different heat inputs, the temperature variation patterns at each measurement point are consistent, following a sequence of "rapid increase → gradual increase → rapid decrease → gradual decrease → stabilization". During the entire process, when Q is 0.77 J·min^{-1}, the T_{max} at the fire source point is the highest. When Q is 0.35, 0.27, and 0.26 J·min^{-1}, the T_{max} at the fire source point is lower than the T_{max} at measurement point 2. Combined with Figure 1, it can be observed that when Q is less than 0.35 J·min^{-1}, the flame size increases sharply, the fire source point is heated by the flame center and the #2 temperature measurement point is heated by the outer flame. The outer flame is a part with sufficient oxygen, which burns more completely and generates more heat, so the temperature is higher. In contrast, the inner flame is usually located in the center of the flame, and the temperature is relatively low due to insufficient oxygen supply.

3. Temperature test results and analysis

3.1. The temperature-time curves of different measurement points

The temperature measurement results for test plates #1, #2, #3, and #4 are shown in Fig. 3.

3.2. The peak temperature T_{max} at the temperature measurement point

The statistical results of the peak temperatures at each measurement point on the four test boards are shown in Fig. 4.

From Fig. 4, it can be observed that the peak temperature variation pattern along the rolling direction is the same for the

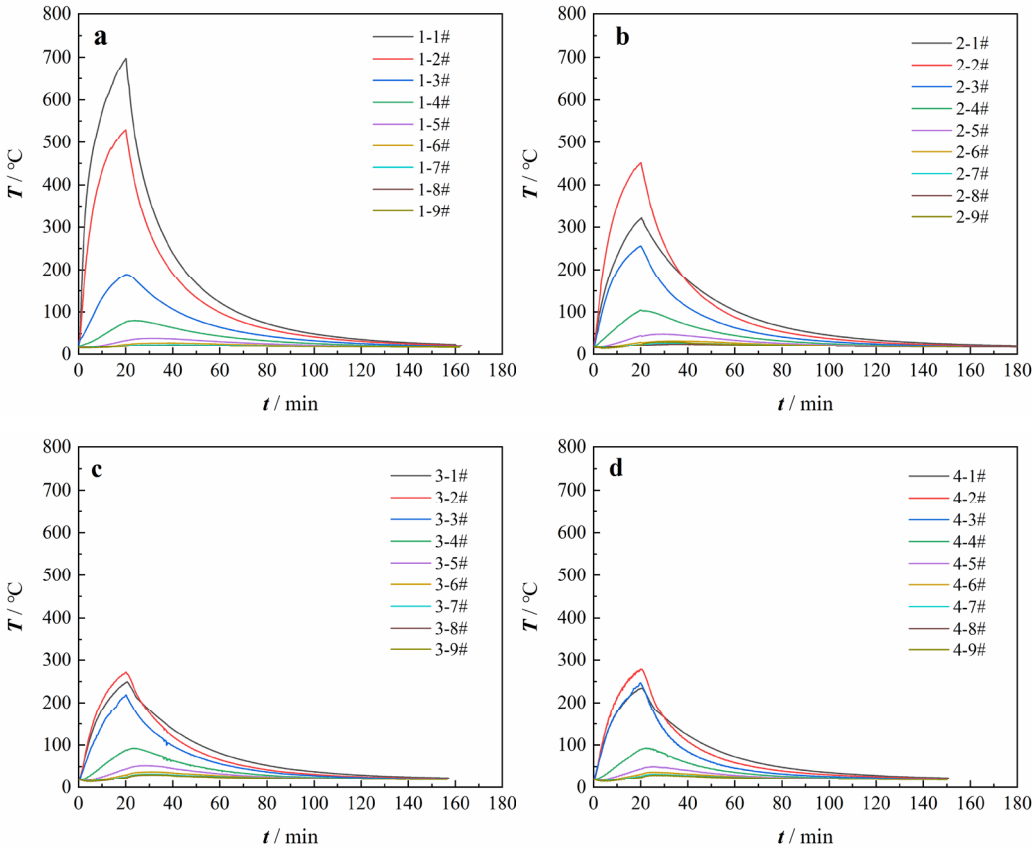

Fig. 3. The temperature-time relationship curves of 9 temperature measuring points on each test plate, (a) #1 plate – 0.77 J·min^{-1}; (b) #2 plate – 0.35 J·min^{-1}; (c) #3 plate – 0.27 J·min^{-1}; (d) #4 plate – 0.26 J·min^{-1}

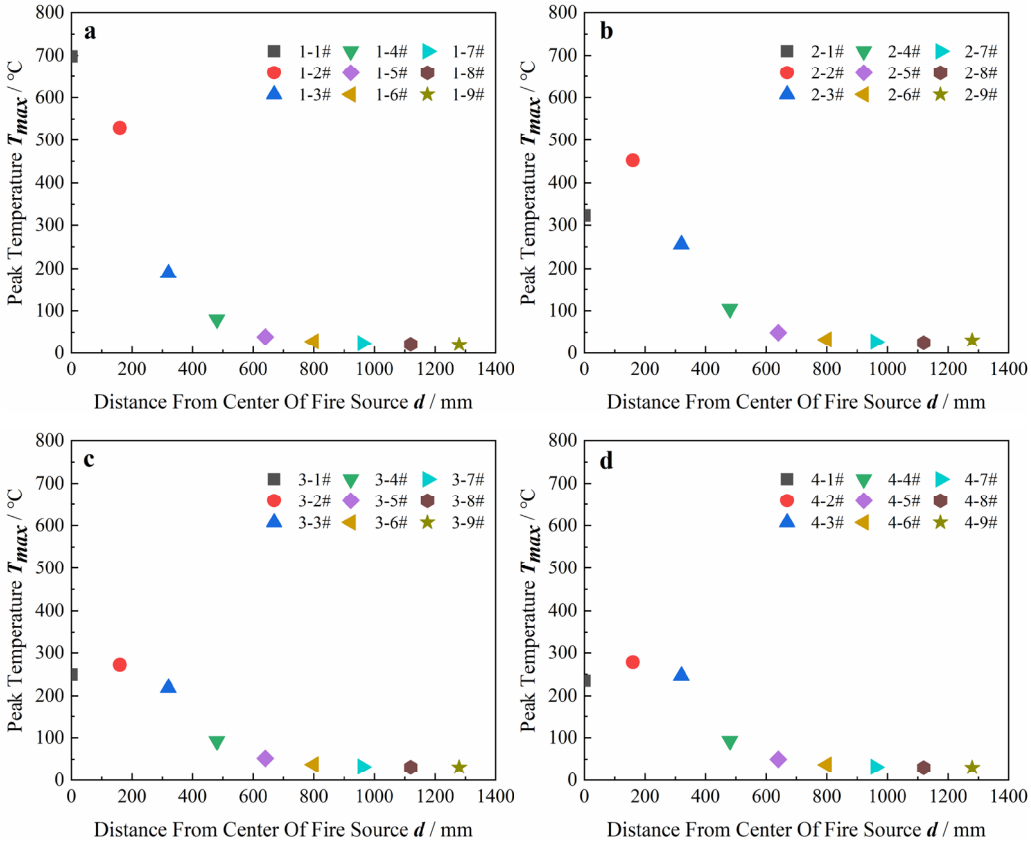

Fig. 4. Statistical results of peak temperature at different temperature measuring points on each test plate, (a) #1 plate – 0.77 J·min^{-1}; (b) #2 plate – 0.35 J·min^{-1}; (c) #3 plate – 0.27 J·min^{-1}; (d) #4 plate – 0.26 J·min^{-1}

four test plates. They all undergo a temperature change process of "gradual decrease → rapid decrease → stabilization". When within 600 mm of the fire source point, the temperature of the steel plate rises significantly; when beyond 600 mm from the fire source point, the temperature increase of the steel plate is not obvious and tends to stabilize. This is because the temperature at the heating end is higher than that at the cold end during the heating process of the steel plate, resulting in a temperature gradient. The heat is transferred from the high temperature zone to the low temperature zone, which makes the cold end gradually warm up. The reason for the lower peak temperature beyond 600 mm from the fire source point is that the steel plate has not reached thermal equilibrium by the end of the heating phase before entering the cooling phase.

3.3. Results of the time required for the temperature measurement point to reach the peak temperature t_{max}

The statistical results of the time taken for each measurement point on the four test plates to reach the peak temperature are shown in Fig. 5.

From Fig. 5, it can be observed that the variation trend of t_{max} along the rolling direction is the same for the four test plates as the distance d increases. As d increases, t_{max} gradually increases and tends to stabilize. The t_{max} values for measurement points # 1 to #3 on each test plates are almost the same, with slightly longer insulation duration, ranging between 20 minutes and 21 minutes. Compared to the insulation duration, the t_{max} values for measurement points #4 to #6 significantly increase, with the magnitude of increase positively correlated with heat input Q. The plate #4 has the smallest increase of about 26.9% and the plate #1 has the largest increase of 91.0%; From the 6th measurement point onwards, the t_{max} of each temperature measurement point tends to be stable.

4. Analysis of the changing characteristics of non-uniform temperature field under different heat inputs

To reveal the characteristics of the non-uniform temperature field variation of steel plates during gas fire incidents, the average rate of temperature change for each temperature point during the heating and cooling stages was statistically analyzed.

4.1. Analysis of temperature field changes during the heating stage

The statistical results of the average heating rate v_r for each temperature point during the heating stage of the four steel plates are shown in Fig. 6.

From Fig. 6, it can be observed that the average heating rate v_r for each plate during the heating stage decreases as the

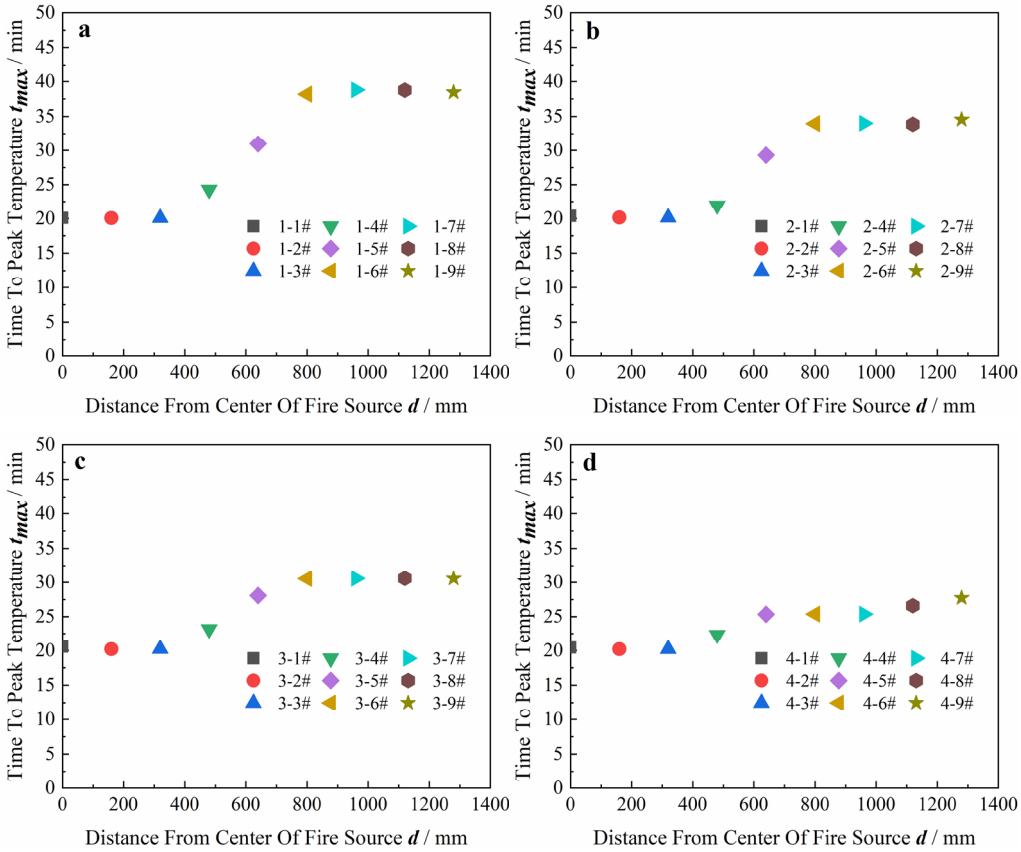

Fig. 5. Statistical results of the time required for each temperature measurement point to reach the peak temperature, (a) #1 plate – 0.77 J·min^{-1}; (b) #2 plate – 0.35 J·min^{-1}; (c) #3 plate – 0.27 J·min^{-1}; (d) #4 plate – 0.26 J·min^{-1}

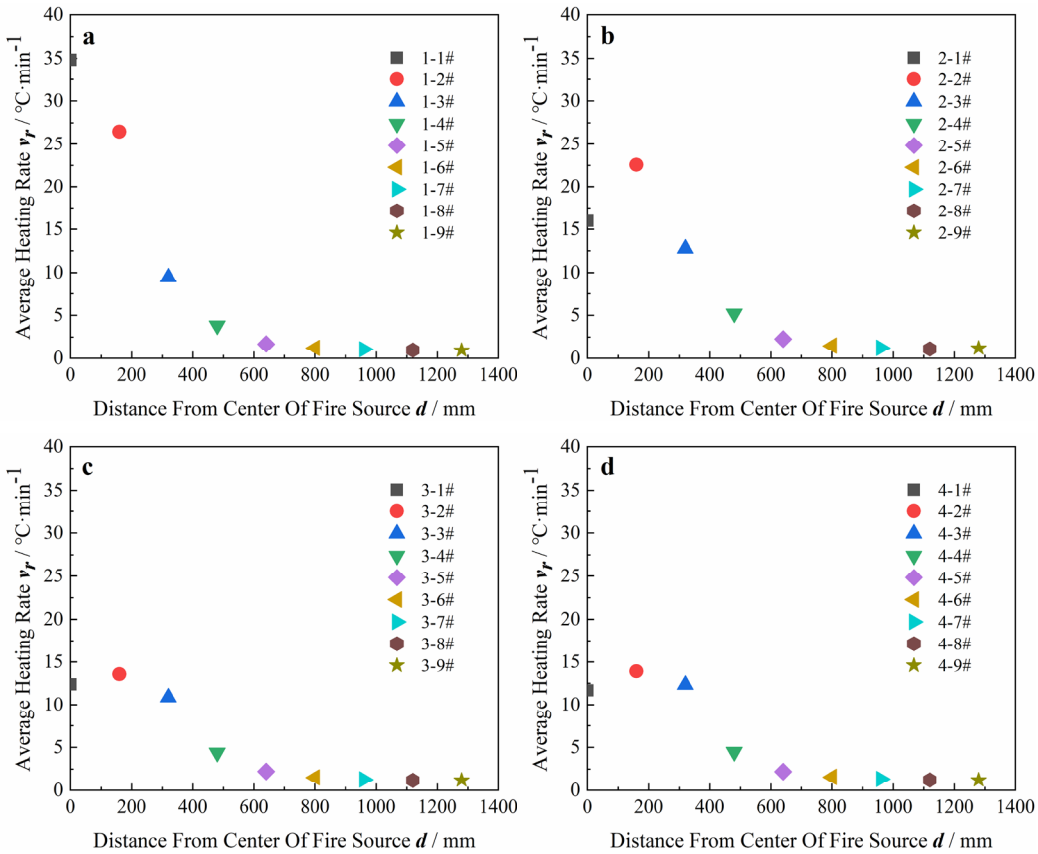

Fig. 6. shows the average rate of temperature increase for each test plate, (a) #1 plate – 0.77 J·min^{-1}; (b) #2 plate – 0.35 J·min^{-1}; (c) #3 plate – 0.27 J·min^{-1}; (d) #4 plate – 0.26 J·min^{-1}

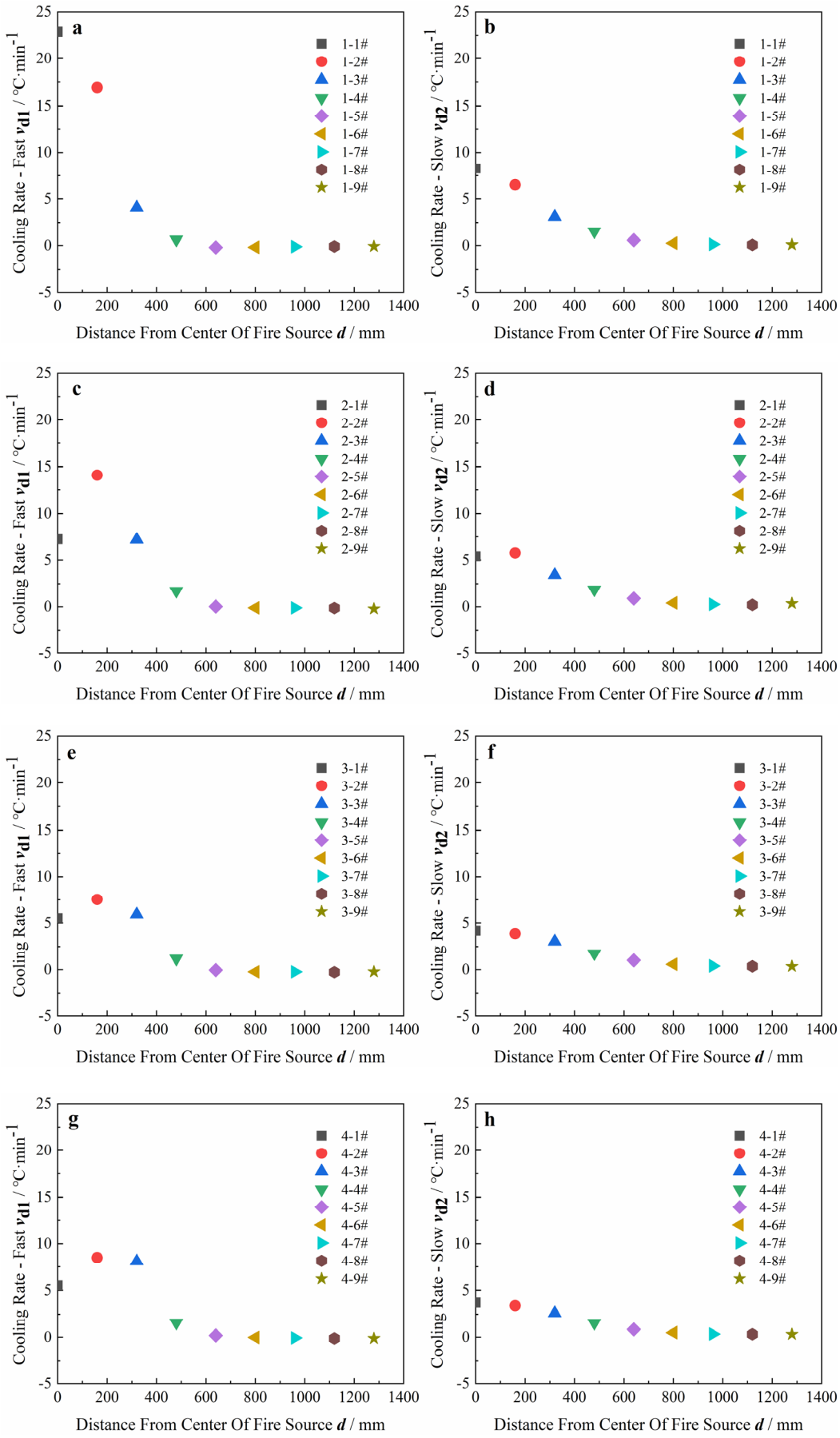

Fig. 7. The rate of temperature decrease during the slow cooling phase for each test plate, (a) #1 plate – 0.77 J·min^{-1} – fast; (b) #1 plate – 0.77 J·min^{-1} – slow; (c) #2 plate – 0.35 J·min^{-1} – fast; (d) #2 plate – 0.35 J·min^{-1} – slow; (e) #3 plate – 0.27 J·min^{-1} – fast; (f) #3 plate – 0.27 J·min^{-1} – slow; (g) #4 plate – 0.26 J·min^{-1} – fast; (h) #4 plate – 0.26 J·min^{-1} – slow

distance d increases. According to Section 3.1, this is due to the fact that during the heating process of the steel plate, the temperature at the heating end is higher than that at the cold end, which creates a temperature gradient that causes v_r to decrease as d increases.

The larger the heat input Q, the higher the v_r at the fire source. When Q is equal to 0.77 J·min^{-1}, 0.35 J·min^{-1}, 0.27 J·min^{-1}, and 0.26 J·min^{-1}, the heating rate v_r at the fire source for each plate is 34.83°C·min^{-1}, 15.96°C·min^{-1}, 12.37°C·min^{-1}, and 11.69°C·min^{-1}, respectively. This is consistent with the relationship between Q and v_r in Formula (1).

4.2. Analysis of temperature field variation characteristics in cooling stage

Considering that the cooling stage of the fire incident can be divided into rapid cooling and slow cooling processes, the statistical results of the average cooling rates v_{d1} and v_{d2} for each temperature measurement point of the four test plates during these two processes are shown in Fig. 7.

From Fig. 7, it can be observed that the average cooling rates v_{d1} and v_{d2} for each test plate decrease as the distance d increases. During the rapid cooling stage, when Q is equal to 0.77 J·min^{-1}, 0.35 J·min^{-1}, 0.27 J·min^{-1}, and 0.26 J·min^{-1}, the maximum cooling rates are 22.88°C·min^{-1}, 14.06°C·min^{-1}, 7.54°C·min^{-1}, and 8.50°C·min^{-1}, respectively. During the slow cooling stage, the maximum cooling rates do not exceed 5°C·min^{-1} for all test boards.

5. The non-uniform temperature distribution pattern of peak temperature

5.1. The distribution pattern of peak temperature for Q355B steel plate under gas fire conditions

To reveal the non-uniform distribution pattern of the temperature field of Q355B steel plate under thermal gas fires, a statistical method is adopted to analyze the peak temperatures at each temperature measurement point on each plate. Considering that the temperature field distribution patterns on all plates are the same and follow the Boltzmann function (Formula (2)), the Boltzmann function is used to fit the peak temperatures at each measurement point on each plate. The fitting results are shown in Fig. 8.

$$T = \frac{T_i - T_f}{1 + e^{\frac{d - d_0}{c}}} + T_f \tag{2}$$

where T_i – initial temperature, in °C; T_f – final temperature, in °C; d – distance from the center of the fire source, in mm; d_0 – distance at which T equal $\frac{T_i + T_f}{2}$ in mm; c – distance constant, in mm; T – peak temperature, in °C.

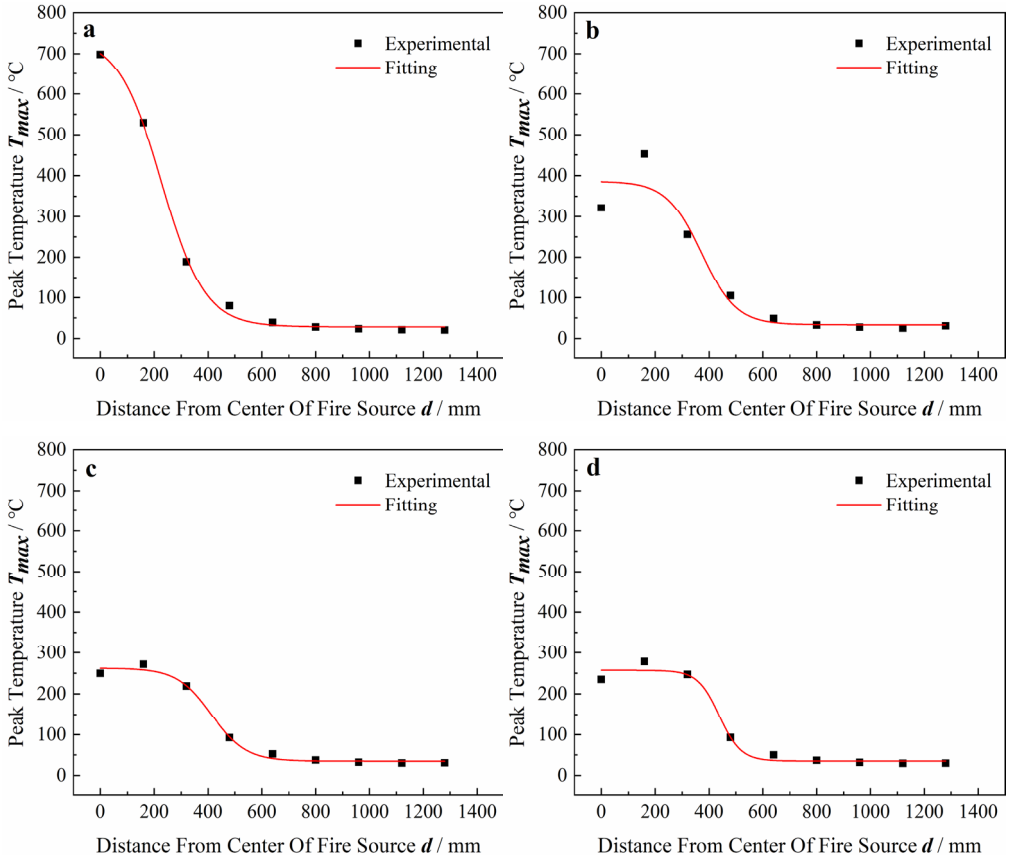

Fig. 8. The distribution patterns of peak temperatures for each test plate under different heat inputs, (a) #1 plate – 0.77 J·min^{-1}; (b) #2 plate – 0.35 J·min^{-1}; (c) #3 plate – 0.27 J·min^{-1}; (d) #4 plate – 0.26 J·min^{-1}

TABLE 3 presents the fitting results of the five parameters T_i, T_f, T_i-T_f(ΔT), d_0, and c in Fig. 8. Among these parameters, T_i, ΔT and d_0 have a significant impact on the peak temperature T_{max}, while T_f and c have a smaller influence on T_{max}. To elucidate the relationship between the peak temperature T_{max} and the heat input Q, an analysis was conducted of the relationship between Q and the five fitting parameters.

TABLE 3

The statistical results of characteristic parameters for gas fire tests on each test plate

Test plate number	#1	#2	#3	#4
T_i / °C	740.91	386.00	262.19	256.98
T_f / °C	28.46	33.52	35.02	35.34
$\Delta T = T_i - T_f$	712.45	352.48	227.17	221.64
d_0 / mm	226.83	372.32	413.61	438.47
c / mm	80.93	64.48	64.02	40.32

5.2. The non-uniform distribution model of peak temperature for Q355B steel plate under gas fire condition

The relationship between heat input Q and the characteristic parameters referring to ΔT, d_0, c and T_f given in TABLE 3 are shown in Fig 9.

From Fig. 9, it can be observed that Q shows a linear relationship with ΔT, while Q exhibits an exponential function relationship with d_0. Since there is not much variation in T_f and c of different heat inputs Q, the average values of T_f and c for each test plate can be taken as the general results for the distribution model of the peak temperature T_{max}.

By combining TABLE 3 and Formula (2), the linear relationship between ΔT and Q, and the exponential relationship between d_0 and Q, one can derive a non-uniform distribution model for the peak temperature T_{max} in a gas fire. This model can be represented by:

$$\begin{cases} T_{max} = \dfrac{\Delta T}{1+e^{\frac{d-d_0}{62.44}}} + 33.09 \\ \Delta T = 949.93Q - 13.41, \quad R^2 = 0.9855 \\ d_0 = 553.09e^{\frac{-Q}{0.36}} + 161.72, \quad R^2 = 0.9825 \end{cases} \tag{3}$$

In Eq. (3): T_{max} – peak temperature, in °C; d – distance from the fire source point, in mm; ΔT – difference between the initial temperature T_i and the final temperature T_f, in °C; d_0 – distance at which T equals $\frac{T_i + T_f}{2}$ in mm.

To validate the reliability of Formula (3), experimental values of T_{max} at fire source points #1 to #4 are taken, and ex-

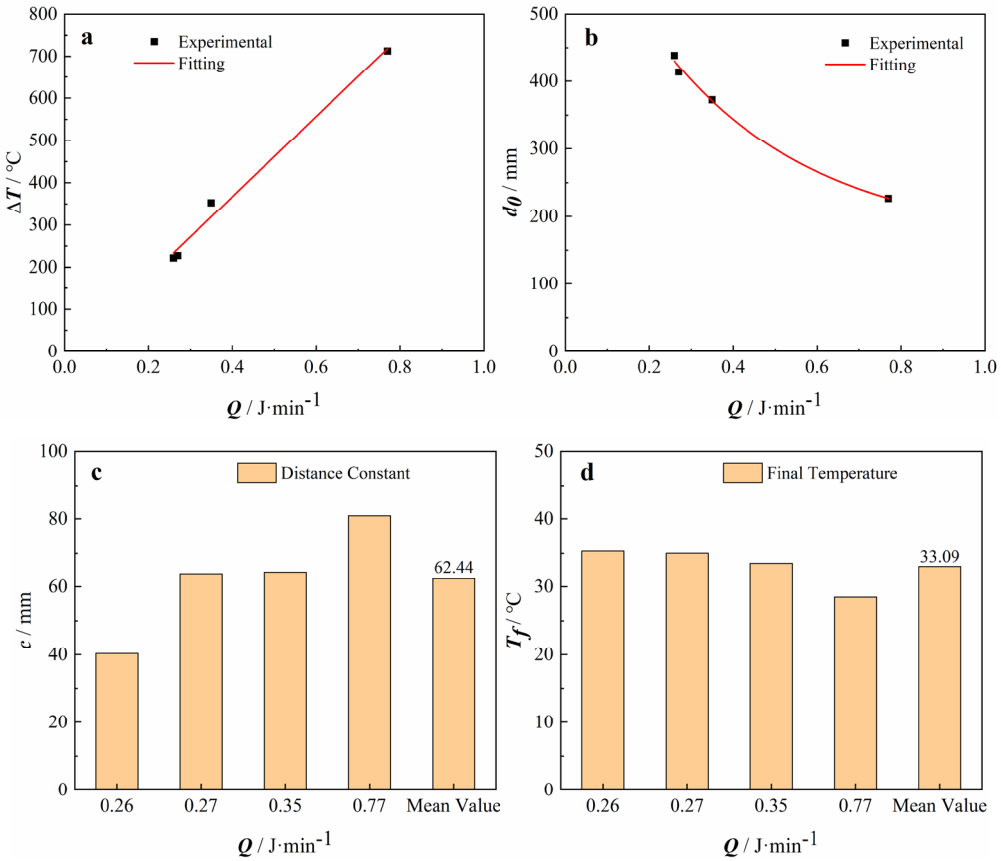

Fig. 9. The relationship between heat input and the characteristic parameters of the experiment, (a) Heat input Q-ΔT (b) Heat input Q-d_0; (c) Heat input Q-c; (d) Heat input Q-T_f

periments were conducted on four test plates. The comparison between the experimentally obtained T_{max} values at the fire source points and the calculated values using Formula (3) is shown in Fig. 10.

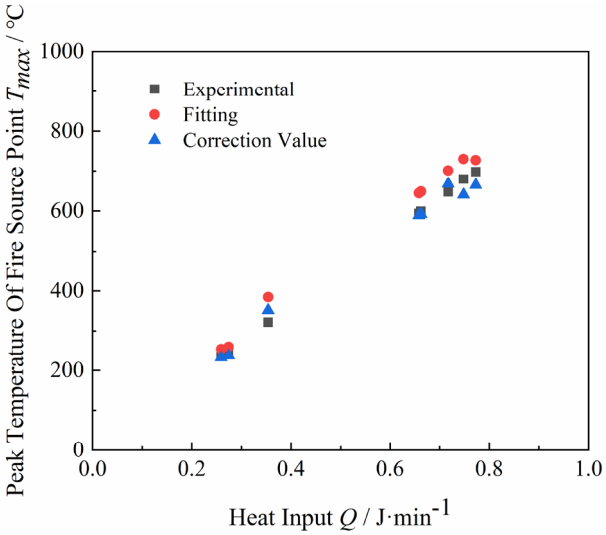

Fig. 10. T_{max} error correction

From Fig. 10, it can be observed that the T_{max} values calculated using Formula (3) are consistently higher than the experimental values, with an average overestimation of 8.64%. In order to further improve the accuracy of T_{max} calculation, a correction is applied to Formula (3) by introducing a modification factor of 0.91. The modified result can be seen in Formula (4). According to Fig. 10, the average deviation is –0.7%.

$$T_{max} = \frac{0.91\Delta T}{1+e^{\frac{d-d_0}{62.44}}} + 30.23 \quad (4)$$

6. Conclusions

The paper investigates the temperature distribution characteristics of grain storage steel during the fire incidents, revealing the temperature distribution features of the grain storage steel in fires. The main conclusions are as follows:

(1) The temperature changes significantly within a distance of 600 mm from the flame point. T_{max} gradually decreases as the distance from the fire source increases. The temperature changes beyond 600 mm are not sensitive. The peak temperature T_{max} at each test plate's fire source point linearly increases with the increase of heat input Q at the fire source.

(2) With the increase of distance d, the change trend of t_{max} in the rolling direction is the same for each test plate. As d increases, t_{max} gradually increases and tends to stabilize. The #4 plate has the smallest increase, approximately 26.9%, while the #1 plate has the largest increase, reaching 91.0%. Starting from the 6th temperature measurement point, t_{max} tends to stabilize for each measurement point.

(3) During the heating stage, the average heating rate v_r of each plate decreases with the increase of d. The larger the Q, the greater the v_r at the fire source. The heating rate v_r at each plate's fire source point linearly increases with the increase of the heat input Q at the fire source.

(4) The average cooling rates v_{d1} and v_{d2} of each test plate decrease with the increase of d. The maximum cooling rates of each test plate in the rapid cooling stage range from 8.50 to 22.88°C·min^{-1}. In the slow cooling stage, the maximum cooling rates do not exceed 5°C·min^{-1}.

Acknowledgements

This work was funded by Anhui University Science Research Projects (2022AH051630 and KJ2021ZD0111), and Bengbu Technology Plan Project (2022hm06), respectively.

REFERENCES

[1] G. Shi, S.H. Wang, C.X. Rong, Experimental investigation into mechanical properties of Q345 steel after fire. J. Constr. Steel. Res. **199**, 107582 (2022). DOI: https://doi.org/10.1016/J.JCSR.2022.107582

[2] D. Huang, L.B. Zhang, W.Y. Wang, H.L Mu, Test on post-fire residual mechanical properties of high strength Q690 steel considering tensile stress in fire. J. Constr. Steel. Res. **194**, 107340 (2022). DOI: https://doi.org/10.1016/j.jcsr.2022.107340

[3] C. Ren, H.X. Wang, Y. Huang, Q. Yu, Post-fire mechanical properties of corroded grade D36 marine steel. Constr. Build. Mater. **263**, 120120 (2020). DOI: https://doi.org/10.1016/j.conbuildmat.2020.120120

[4] L. Shen, M. Ding, W.C. Yao, B. Yang, et al., Post-fire mechanical response of Q960E ultra-high-strength structural steel. J. Constr. Steel. Res. **201**, 107729 (2023). DOI: https://doi.org/10.1016/J.JCSR.2022.107729

[5] Y. Huang, B. Young, Mechanical properties of lean duplex stainless steel at post-fire condition. Thin. Wall. Struct. **130**, 564-576 (2018). DOI: https://doi.org/10.1016/j.tws.2018.06.018

[6] T. Shnal, S. Pozdieiev, O. Nuianzin, S. Sidnei, Improvement of the Assessment Method for Fire Resistance of Steel Structures in the Temperature Regime of Fire under Realistic Conditions. Mater. Sci. Forum. **6123**, 107-116 (2020). DOI: https://doi.org/10.4028/www.scientific.net/MSF.1006.107

[7] X.J. Huang, K. Bi, X.S. Liu, et al., A Model for Predicting Temperature Produced by Upward Spreading Cable Fire under Natural Ventilation. Energy. Procedia **66**, 177-180 (2015). DOI: https://doi.org/10.1016/j.egypro.2015.02.010

[8] X.Q. Wu, T. Huang, K.T.F. Au, J. Li, A Localized Fire Model for Predicting the Surface Temperature of Box Girder Bridges Subjected to Tanker Truck Fire. Fire. Technol. **56**, 2059-2087 (2020). DOI: https://doi.org/10.1007/s10694-020-00966-2

[9] E.Z. Yan, Y.M. Sun, Study on the Distribution of Fire Temperature Field of L-type Cable Corridor through Numerical Simulation. Procedia. Eng. **211**, 861-870 (2018).
DOI: https://doi.org/10.1016/j.proeng.2017.12.085

[10] M.A. Li, Z.P. Wang, Z. Xing, X.M. Song, Numerical Simulation on Temperature Field of Long Narrow Confined Space Fire under Negative Pressure Ventilation Condition. Procedia. Eng. **52**, 272-276 (2013).
DOI: https://doi.org/10.1016/j.proeng.2013.02.139

[11] K.A.M. Moinuddin, S.J. Al-Menhali, K. Prasannan, I.R. Thomas, Rise in structural steel temperatures during ISO 9705 room fires. Fire. Safety. J. **46** (8), 480-496 (2011).
DOI: https://doi.org/10.1016/j.firesaf.2011.08.001

[12] G. Liu, H.G. Meng, G.H. Qu, L. Wang, H.S. Lu, Real-time monitoring and prediction method of commercial building fire temperature field based on distributed optical fiber sensor temperature measurement system. J. Build. Eng. **70**, 106403 (2023).
DOI: https://doi.org/10.1016/J.JOBE.2023.106403

[13] A. Krzemień, Fire risk prevention in underground coal gasification (UCG) within active mines: Temperature forecast by means of MARS models. Energy **170**, 777-790 (2019).
DOI: https://doi.org/10.1016/j.energy.2018.12.179

[14] G.W. Zhang, H.X. Li, G.Q. Zhu, J.Y. Li, Temperature fields for fire resistance analysis of structures exposed to natural fires in large space buildings. Struct. Des. Tall Spec. Build. **29** (4), 1708 (2020). DOI: https://doi.org/10.1002/tal.1708

[15] S. Kim, J. Shim, Y.J. Rhee, D. Jung, C. Park, Temperature Distribution Characteristics of Concrete during Fire Occurrence in a Tunnel. Appl. Sci. **9** (22), 4740 (2019).
DOI: https://doi.org/10.3390/app9224740

[16] O. Nuianzin, M. Kryshtal, A. Nesterenko, et al., Investigation of the regularities of temperature regime of fire in cable tunnels depending on its parameters. MATEC. Web. Conf. **230**, 02002 (2018).
DOI: https://doi.org/10.1051/matecconf/201823002022

[17] X. Xu, G.Q. Zhu, X.J. Zhang, et al., Numerical study on temperature distribution of tunnel structure in fires. Case. Stud. Therm. Eng. **25**, 100874 (2021).
DOI: https://doi.org/10.1016/J.CSITE.2021.100874

[18] X.L. Zhao, C.G. Chen, C.L. Shi, et al., An extended model for predicting the temperature distribution of large area fire ascribed to multiple fuel source in tunnel. Tunn. Undergr. Space. Technol. **85**, 252-258 (2019).
DOI: https://doi.org/10.1016/j.tust.2018.12.013

[19] Y. Jia, X.L. Fan, X.J. Zhao, et al., Study on the longitudinal ceiling temperature distribution induced by double pool fires in a tunnel. Int. J. Therm. Sci. **168**, 107059 (2021).
DOI: https://doi.org/10.1016/j.ijthermalsci.2021.107059

[20] S. Takeuchi, T. Aoki, F. Tanaka, K.A.M. Moinuddin, Modeling for predicting the temperature distribution of smoke during a fire in an underground road tunnel with vertical shafts. Fire. Safety. J. **91**, 312-319 (2017).
DOI: https://doi.org/10.1016/j.firesaf.2017.03.063

[21] J. Li, X. K. Yao, J.Y. Dai, Y.L, Song, Research on Influence and Prediction Model of Urban Traffic Link Tunnel curvature on Fire Temperature Based on Pyrosim – SPSS Multiple Regression Analysis. IOP Conf. Ser.: Earth Environ. Sci. **153** (6), 062032-062032 (2018).
DOI: https://doi.org/10.1088/1755-1315/153/6/062032

[22] L. He, Z.S. Xu, H.G. Chen, et al., Analysis of entrainment phenomenon near mechanical exhaust vent and a prediction model for smoke temperature in tunnel fire. Tunn. Undergr. Space. Technol. **80**, 143-150 (2018).
DOI: https://doi.org/10.1016/j.tust.2018.06.011

[23] E.C. Fischer, A.H. Varma, J.A. Gordon, Performance-Based Structural Fire Engineering of Steel Building Structures: Traveling Fires. Front. Built. Environ **8**, 907237 (2022).
DOI: https://doi.org/10.3389/fbuil.2022.907237

[24] Charlier. Marion, F. JeanMarc, D. Fabien. N. Ali, V. Olivier, Development of an Analytical Model to Determine the Heat Fluxes to a Structural Element Due to a Travelling Fire. Appl. Sci. **11** (19), 9263-9263 (2021). DOI: https://doi.org/10.3390/APP11199263

[25] X. Yan, G. Thomas, Numerical modeling of localized fire exposures on structures using FDS-FEM and simple models. Eng. Struct. **246**, 112997 (2021).
DOI: https://doi.org/10.1016/j.engstruct.2021.112997

[26] Ren. Chong, P. Zhang, S. Yan, L.S. Dai, Analysis and design of cold-formed steel storage rack uprights under localised fires. Structures **27**, 2082-2095 (2020).
DOI: https://doi.org/10.1016/j.istruc.2020.08.022

[27] B.C. Xie, J. Hou, G. B. Lou, et al., Experimental and numerical investigation on temperature field of stainless-steel core plate exposed to fire considering cavity radiation effects. Thin. Wall. Struct. **163**, 107695 (2021).
DOI: https://doi.org/10.1016/j.tws.2021.107695

[28] G. Wu, X. Wang, X.B. Xie, et al., Temperature Distribution Characteristics of Steel Circular Tube Members under Oil Pool Fire Conditions: Experiment and Numerical Simulation. Int. J. Thermophys. **42** (8), 114 (2021).
DOI: https://doi.org/10.1007/S10765-021-02866-1

[29] H. Sadiq, M.B. Wong, J. Tashan, et al., Determination of Steel Emissivity for the Temperature Prediction of Structural Steel Members in Fire. J. Mater. Civil. Eng. **25** (2), 167-173 (2013).
DOI: https://doi.org/10.1061/(asce)mt.1943-5533.0000607

[30] GB 51249-2017, Code for fire safety of steel structures in buildings.